Acta Crystallographica Section D
Biological Crystallography
ISSN 0907-4449

MAD phasing with krypton

Aina Cohen,[a] Paul Ellis,[a] Nicole Kresge[b] and S. Michael Soltis[a]*

[a]The Stanford Synchrotron Research Laboratory, SLAC, PO Box 4349, Bin 99, Stanford University, CA 94309, USA, and [b]The Scripps Research Institute, Department of Molecular Biology, 10550 North Torrey Pines Road, La Jolla, CA 92037,USA

Correspondence e-mail: soltis@slac.stanford.edu

Received 20 June 2000
Accepted 18 October 2000

Experiments demonstrating the feasibility of Kr-edge MAD on frozen crystals as a routine method for structure determination are reported. Approximately 50% of protein crystals can be successfully derivatized by pressurization with the noble gases xenon or krypton. While Xe has produced many useful derivatives for MIR phasing over the last several years, the Xe edges (*K* edge = 34.6 keV, $L_{\rm I}$ = 5.5 keV) are not easily accessible for MAD studies. As the Kr *K* edge (14.3 keV) is accessible on most MAD beamlines, Kr derivatization provides the additional opportunity to conduct a MAD experiment and obtain phases using only a single crystal. This paper describes the phasing of two proteins using Kr MAD: the 17 kDa Fe protein myoglobin (Mb) from sperm whale (*Physeter catodon*) and an 18 kDa protein (SP18) from green abalone (*Haliotis fulgens*). Three-wavelength data were collected at SSRL beamline 9-2 from crystals of Mb and SP18 incubated in 2.76 MPa of Kr gas for 2 min, depressurized and then flash-frozen in a stream of nitrogen gas at 100 K. MAD phases were calculated using the program *SHARP* and the resulting density improved with *wARP*. The final maps for both Mb and SP18 were of excellent quality.

1. Introduction

For many protein crystals, pressurization with the noble gases xenon and krypton can be an easy method for introducing a heavy atom into the structure. Using Xe, this method has been shown to be approximately 50% effective (Stowell *et al.*, 1996). While there is less experience with Kr, it has generally been observed to bind in the same sites as Xe, although higher pressures may be required to achieve the same occupancy (Schiltz, Shepard *et al.*, 1997).

Xe and Kr derivatization can be complementary to more traditional methods. Xe prefers hydrophobic cavities but has also been observed to bind in a variety of other environments (Prangé *et al.*, 1998). These sites tend to be unique compared with those occupied by more conventional heavy-atom compounds. Unlike derivatives produced by co-crystallization or soaking, Xe derivatives tend to be extremely isomorphous to native crystals and the extent of binding may be controlled by changing the pressure (Tilton *et al.*, 1984).

The use of Xe derivatives has become more routine as specialized apparatus has become available. The first room-temperature devices (Schoenborn *et al.*, 1965; Tilton *et al.*, 1984; Tilton, 1988; Kroeger & Kundrot, 1994; Schiltz *et al.*, 1994; Stowell *et al.*, 1996) pressurized the crystal in a glass capillary up to 10 MPa of gas. However, there were potential problems with this technique, including limited crystal lifetimes at room temperature, background scatter from excess

Xe, the formation of xenon hydrates and the risk of capillary explosion. Later, Soltis *et al.* (1997) devised a simple device for the production of cryocooled Xe and Kr derivatives, removing the necessity for the capillary. More recently, commercial models such as the Cryo-Xe-Siter (Sauer *et al.*, 1997) from Molecular Structure Corporation (Texas, USA), the Xcell (Djinovic Carugo *et al.*, 1998) from Oxford Cryosystems (Oxford, England) and the Xenon Chamber from Hampton Research (Machius *et al.*, 1999) have appeared. The Cryo-Xe-Siter has the additional advantage of allowing the crystal to be cryocooled while still under pressure, thereby maximizing the occupancy of the heavy atom in the crystal.

A single Xe derivative is not typically sufficient to phase a macromolecular crystal structure. Rather, it is generally used as just one of a number of derivatives for the MIR or MIRAS method. Because there are experimental difficulties working at the absorption edges of Xe, the multi-wavelength anomalous dispersion (MAD) technique has not been routinely used. At the Xe *L* edge (5.5 keV, 2.3 Å), significant absorption typically prevents the extraction of reliable phases. At the *K* edge (34.6 keV, 0.36 Å), the diffraction pattern is significantly contracted and the energy is not generally accessible on many MAD synchrotron beamlines. Schiltz, Kvick *et al.* (1997) have reported the successful collection of anomalous data above the Xe *K* edge; however, this method has not been widely utilized.

As the Kr *K* edge (14.3 keV, 0.87 Å) is readily accessible on most MAD synchrotron beamlines, Kr derivatization provides the opportunity to conduct a MAD experiment and obtain phases using only a single crystal. This paper describes the phasing of two proteins using Kr MAD: the 17 kDa Fe protein myoglobin (Mb) from sperm whale (*P. catodon*) and an 18 kDa protein (SP18) from green abalone (*H. fulgens*). We chose to study Mb because it was readily available and has a well characterized Xe derivative (Schoenborn *et al.*, 1965; Schoenborn, 1969; Tilton *et al.*, 1984; Vitali *et al.*, 1991) with one major and three minor binding sites. SP18 was chosen because it was also known to bind xenon and unlike Mb contains no endogenous anomalous scatterers. The structure of this protein has previously been determined (Kresge *et al.*, in preparation) using the MIR method with five heavy-atom derivatives.

2. Experimental

2.1. Crystallization and crystallographic data for Mb

Recombinant *P*6 Mb solution from Sigma (M-7527) was concentrated to 20 mg ml^{-1} and used without further purification. Crystals of Mb were grown at 295 K using the hanging-drop vapor-diffusion method by equilibration against a reservoir solution containing 2.5 *M* $(NH_4)_2SO_4$, 1 m*M* EDTA and 20 m*M* Tris pH 9.0. The drops were left to equilibrate for one week and then seeded with a solution obtained by crushing a crystal and diluting by a factor of 100.

A crystal of approximately 130 × 80 × 20 µm was mounted in a fiber loop on an SSRL-style mounting pin (Stanford Synchrotron Radiation Laboratory, 2000). The crystal was removed from the mother liquor and immediately dipped in a cryoprotectant solution consisting of a 25% solution of sucrose in the mother liquor. The pin was then placed inside the pressurization cell (Soltis *et al.*, 1997). A small vial of water had already been placed inside the cell to prevent crystal dehydration. The cell was pressurized with 2.76 MPa of Kr gas for 2 min, depressurized and quickly opened. The pin was removed using a magnetic wand and the sample was flash-cooled in a stream of nitrogen gas at 110 K. The elapsed time between depressurization and flash-cooling was approximately 15 s.

Diffraction data at three wavelengths for MAD phasing were collected using an ADSC Quantum-4 CCD detector operated by the software package *BLU-ICE* (Stanford Synchrotron Radiation Laboratory, 2000) at SSRL beamline

Table 1
Processing statistics for the 'standard' and 'extended' MAD data collections for Mb.

	Standard data set			Extended data set		
	Edge	Peak	Remote	Edge	Peak	Remote
X-ray wavelength (Å)	0.8656	0.8644	0.8463	0.8656	0.8644	0.8463
Resolution (Å)	17–1.7	17–1.7	17–1.7	17–1.7	17–1.7	17–1.7
Measured reflections	231993	232331	237805	463161	464013	475177
Unique reflections	23327	23322	23374	23339	23335	23403
Completeness (%)	99.6	99.6	99.8	99.6	99.6	99.8
Anomalous completeness (%)	99.6	99.6	99.8	99.6	99.6	99.8
Multiplicity	9.9	10.0	10.2	19.8	19.9	20.3
$I/\sigma(I)$ (overall)	26.6	26.8	26.4	28.8	28.6	27.9
$I/\sigma(I)$ (1.71–1.70 Å)	11.2	11.5	11.4	10.7	10.9	10.5
$R_{\rm merge}$† (deviation from mean $I+$ or $I-$)	0.065	0.064	0.065	0.091	0.091	0.099

† $R_{\rm merge} = \sum_{hkl,i}|I_{hkl,i} - \langle I_{hkl}\rangle|/\sum_{hkl,i}\langle I_{hkl}\rangle$.

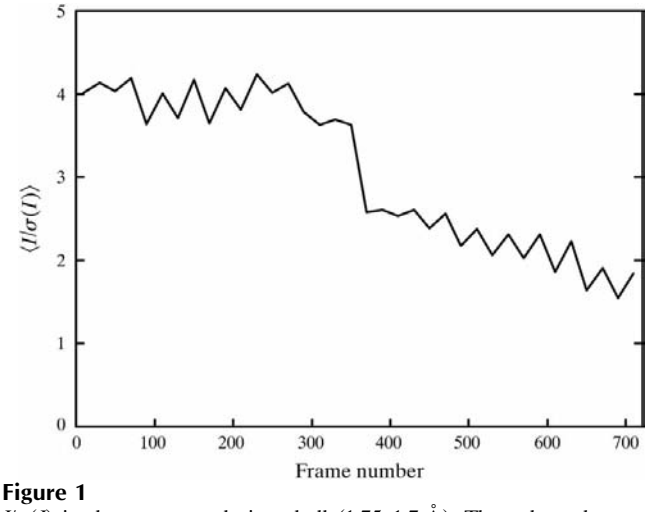

Figure 1
$I/\sigma(I)$ in the outer resolution shell (1.75–1.7 Å). The values shown are averages for sequential groups of 20 images from the peak wavelength data set. Each image represents a 15 s exposure plus a 10 s dead time for detector readout. The step from frame 360 to frame 361 is a consequence of time-dependent crystal decay that occurred during an 8 h idle period between the two data collections. Similar decay has also been observed with Mb crystals not treated with Kr.

Table 2
The fractional coordinates, occupancies (Q), anomalous signal (f'') and B factors of the Kr sites in Mb and SP18 refined using *SHELX*, and the occupancies of the corresponding Xe-sites from the $P2_1$ Mb (Tilton *et al.*, 1984) and SP18 (Kresge *et al.*, in preparation) Xe derivatives.

The parameters of the Fe atom in Mb are also shown.

(*a*) MB.

	Fractional coordinates						Xe-derivative site	
Atom	*a*	*b*	*c*	*Q*	f''	*B* (Å^2)	Atom	*Q*
Kr1	0.383	0.046	0.001	0.68	2.7	22	Xe1	0.94
Kr2	0.476	0.156	0.122	0.28	1.1	19	Xe4	0.46
Kr3	0.415	0.128	0.799	0.17	0.7	12	Xe3	0.48
Kr4	0.382	0.115	0.981	0.08	0.3	26	Xe2	0.57
Fe	0.411	0.051	0.103	1.00	1.2	8		

(*b*) SP18.

	Fractional coordinates						Xe-derivative site	
Atom	*a*	*b*	*c*	*Q*	f''	*B* (Å^2)	Atom	*Q*
Kr	0.134	0.548	0.022	0.42	1.6	44	Xe	0.63

9-2. The wavelengths for data collection were selected using a plot of f' and f'' calculated with the program *CHOOCH* (Evans & Perrifer, 1996) from the X-ray fluorescence spectrum of the crystal. The detector was arbitrarily positioned for a maximum resolution of 1.7 Å, which was judged to be a sufficient resolution for the purposes of the experiment. A test image was collected and indexed with *MOSFLM* (Leslie, 1999). Employing the strategy option, it was determined that 90° of rotation was the minimum required to obtain complete data. Using a rotation angle of 0.5° and an exposure time of 15 s per image, a total of 180° were collected at each wavelength following the inverse-beam method with a wedge size of 10°.

All data were processed using *MOSFLM* (Leslie, 1999) and the programs *SCALA* and *TRUNCATE* from the *CCP*4 program package (Collaborative Computational Project, Number 4, 1994). The crystals obtained belong to the hexagonal space group *P*6, with unit-cell parameters $a = b = 90.4$, $c = 45.3$ Å.

From the decrease in intensity of the higher resolution shells with time (Fig. 1), it was evident that the crystal had begun to decay. In an effort to evaluate whether improved phases could be obtained by collecting further redundant data from a radiation-damaged crystal, the collection was repeated and the additional data combined with the original 'standard' data to form an 'extended' set. A summary of the data collection and reduction statistics is given in Table 1. All subsequent analysis was carried out using both the standard and extended data sets.

2.2. Phase determination for Mb

2.2.1. Phase determination with the 'standard' data set. The two highest peaks in an anomalous difference Patterson synthesis calculated using data collected at the maximum of f'' were 22 and nine times the standard deviation of the map

Table 3
Processing statistics for SP18.

	Edge	Peak	Remote
X-ray wavelength (Å)	0.8653	0.8651	0.8474
Resolution (Å)	24–2.0	24–2.0	22–2.0
Measured reflections	721215	739623	755615
Unique reflections	18874	18879	18882
Completeness (%)	99.6	99.6	99.6
Anomalous completeness (%)	100.0	99.9	99.9
Multiplicity	38.2	39.2	40.0
$I/\sigma(I)$ (overall)	31.0	30.7	30.4
$I/\sigma(I)$ (2.02–2.00 Å)	1.41	1.48	1.47
$R_{\rm merge}$ (deviation from mean *I*+ or *I*–)	0.097	0.101	0.096

(Fig. 2). A search for anomalous scatterers using *CNS* (Brunger *et al.*, 1998) yielded a Kr site corresponding to the 22σ peak as well as the expected heme Fe atom corresponding to the 9σ peak. The parameters of these two atoms were refined against the MAD data in the resolution range 18–1.7 Å using the program *SHARP* (de La Fortelle, 1997). The resulting phase estimates were used to calculate an anomalous difference Fourier map which enabled the location of a minor Kr-binding site. After the addition of this site, the phases were further refined with *SHARP*. The experimental phases were improved using *wARP* (Perrakis *et al.*, 1997).

The quality of the initial phase determination was assessed by comparing the experimental maps with theoretical density from a refined model. A starting model was derived from a mutant *P*6 myoglobin (PDB entry 1dxc; Brunori *et al.*, 2000) by replacing the mutated residues with native using the program *XFIT* from the *XtalView* package (McRee, 1999). Four Kr atoms were also added, comprising the two included in the phasing model and two further minor sites identified in a phased anomalous map. The resulting model was refined with *SHELX* (Sheldrick, 1997) to a final *R* factor of 0.17. The

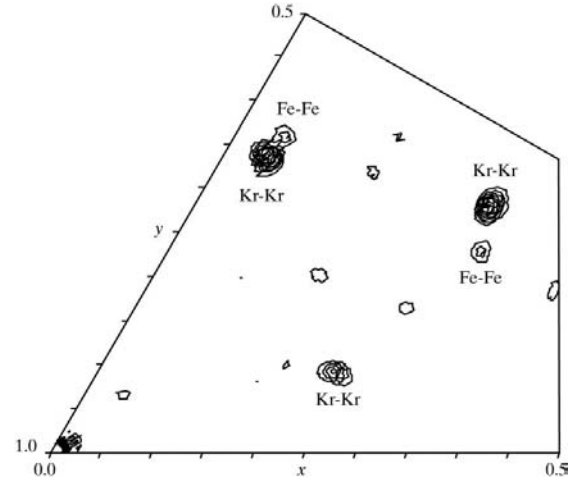

Figure 2
Harker section ($z = 0$) of the Patterson synthesis calculated using the anomalous differences of the standard data set collected at the Kr *K* absorption-edge maximum. The map is contoured in increments of 3σ and the Kr–Kr and Fe–Fe peaks above 6σ are labeled. The figure was prepared using the program *XCONTUR* (McRee, 1999).

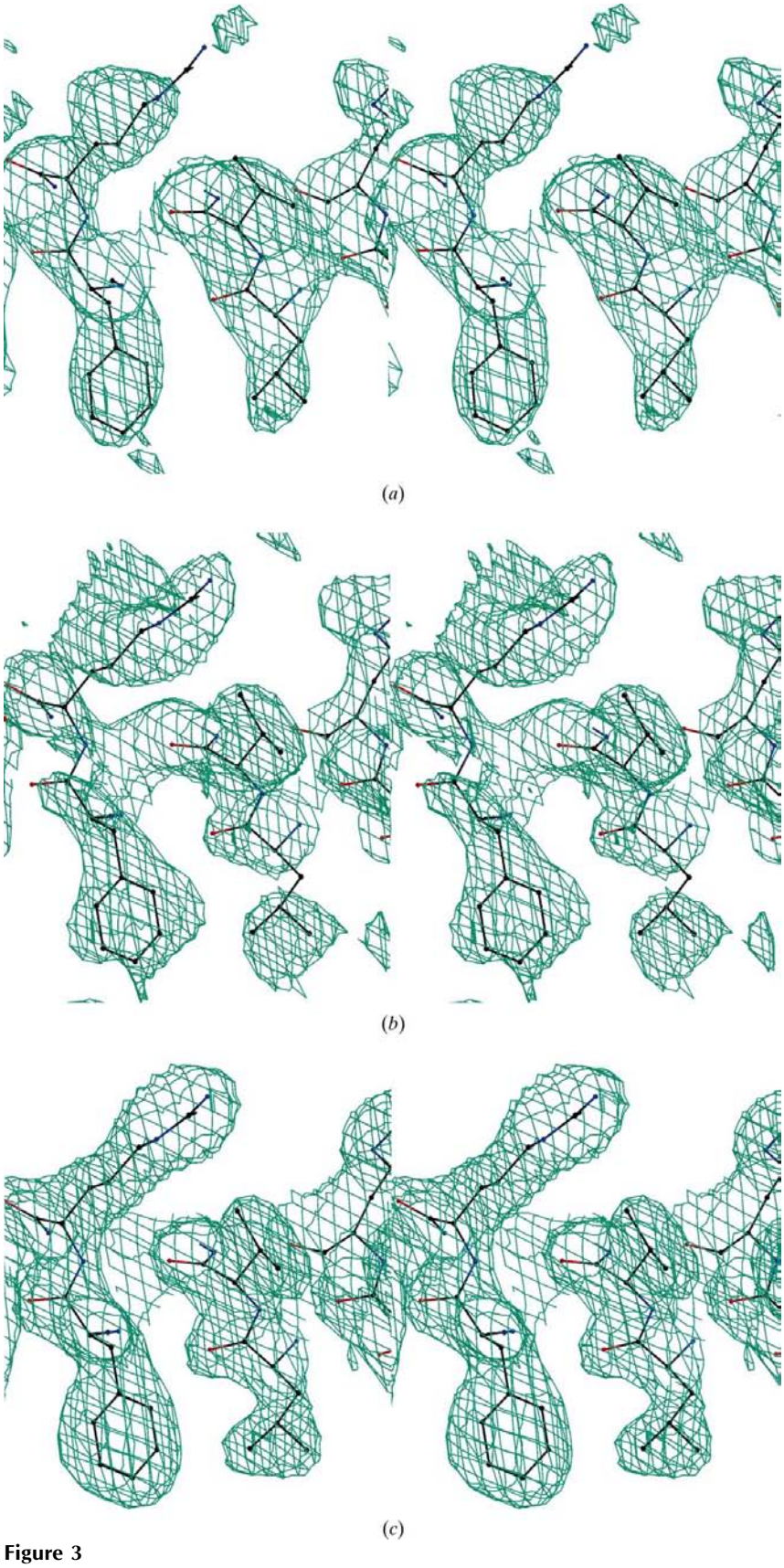

Figure 3
Stereoviews of the raw electron density of SP18 as determined by (*a*) MIR and (*b*) Kr MAD. The Kr MAD density after improvement with *wARP* is shown in (*c*). All maps are contoured at 1σ. The figures were prepared using the programs *XFIT* (McRee, 1999) and *Raster3D* (Merritt & Bacon, 1997).

refined Kr sites and occupancies are listed in Table 2. The real-space correlation between the (F_c, φ_c) map calculated from the model and the 'best' map from *SHARP* was 0.54. After improvement with *wARP* the correlation increased to 0.94.

2.2.2. Phase determination with the 'extended' data set. With the extended data, the two highest peaks in the anomalous difference Patterson synthesis were slightly lower at 20σ and 8σ. Although the phase estimates output from *SHARP* had higher figures of merit (average for all reflections = 0.83) than those from the standard data set (0.64), the real-space correlation between the model and the 'best' map from *SHARP* was only 0.28.

2.3. Crystallization and crystallographic data for SP18

The 18 kDa protein from green abalone was purified by CM cellulose chromatography (Vacquier & Lee, 1993), dialyzed against 50 m*M* sodium acetate pH 4.9 and concentrated to 10 mg ml^{-1}. Crystals were grown at 295 K using the hanging-drop vapor-diffusion method by equilibration against a reservoir solution of 1.0 *M* potassium/sodium tartrate, 100 m*M* *N*-cyclohexyl-2-aminoethanesulfonic acid (CHES) buffer pH 9.5 and 200 m*M* lithium sulfate.

A crystal of approximately 200 × 200 × 100 µm was removed from the mother liquor and immediately dipped in a cryoprotectant solution consisting of mother liquor with 25% ethylene glycol. The crystal was then pressurized with 2.76 MPa of Kr gas for 2 min, depressurized and frozen in the same manner as for the myoglobin sample.

Diffraction data at three wavelengths for MAD phasing were collected using a rotation angle of 0.5° and an exposure time of 15 s per image. A total of 360° were collected at each wavelength following the inverse-beam method with a wedge size of 10°. All data were processed in the same way as for Mb. The crystal belonged to the hexagonal space group $P6_122$, with unit-cell parameters $a = b = 66.8$, $c = 202.7$ Å. A summary of the data-collection and reduction statistics is given in Table 3.

2.4. Phase determination for SP18

A search for anomalous scatterers using *CNS* (Brunger *et al.*, 1998) yielded one Kr site. The parameters of this atom were

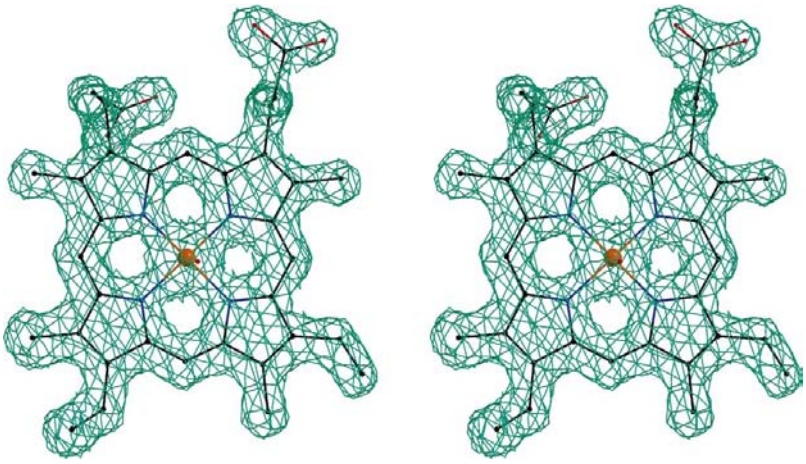

Figure 4
Stereoview of the *wARP*-improved electron density of the heme group in Mb, contoured at the 2σ level. The figure was prepared using the programs *XFIT* (McRee, 1999) and *Raster3D* (Merritt & Bacon, 1997).

refined against the MAD data in the resolution range 20–2.0 Å using the program *SHARP*. The experimental phases were then improved using *wARP*. A starting model, derived from the original MIR structure, was refined with *SHELX* (Sheldrick, 1997) to a final *R* factor of 0.25. The refined Kr site coordinates and occupancy are listed in Table 2. The real-space correlation between the (F_c, φ_c) map calculated from the model and the 'best' map from *SHARP* was 0.51 (compared with 0.60 for the original MIR map). After improvement with *wARP* the correlation increased to 0.86.

3. Results and discussion

The density as determined by Kr MAD from a single crystal of SP18 was comparable with that obtained using MIR with data from five crystals and almost all backbone and side-chain groups were clearly visible in the final map (Fig. 3). Likewise, the *wARP*-improved electron-density map calculated with the 'standard' data set for Mb was of excellent quality (Fig. 4).

In contrast, the density calculated from the 'extended' Mb data was essentially uninterpretable, demonstrating that the potential benefits from high redundancy can easily be offset by the effects of crystal decay. If completeness has been attained, experimenters should therefore be circumspect about adding data from a potentially radiation-damaged crystal.

All four Kr-binding sites in Mb correspond to those occupied by Xe in the Xe derivative of the $P2_1$ form (Tilton *et al.*, 1984) and the single Kr-binding site in SP18 corresponds to the single Xe site (Table 2). As expected, all the sites have lower occupancies than in the corresponding Xe derivative. As this study shows, however, complete binding is not always required, as we were able to successfully phase an 18 kDa protein with only a single 40% occupied site.

Moreover, Kr appears to bind at a faster rate than Xe. Incubation times of up to 15 min yielded no measurable binding of Xe in SP18, whereas in the present study an incubation time of just 2 min was used to incorporate Kr. A shorter incubation time will generally be beneficial to sample quality as the crystal is less likely to be adversely affected by evaporation of the mother liquor. Given the high off-rate for Xe (Soltis *et al.*, 1997) (and presumably also for Kr), a device such as the MSC Cryo-Xe-Siter that allows for cryocooling samples while still under pressure may be expected to produce higher occupancies. We plan to test this hypothesis in the near future.

4. Conclusions

We have shown that Kr *K*-edge MAD on flash-cooled crystals can be a quick and easy method for phasing macromolecular structures despite the generally lower occupancies than with Xe. With the expected 50% success rate of Kr binding in proteins and the increased availability of low-temperature pressure cells at synchrotron facilities, Kr MAD may well become a standard phasing technique.

We would like to thank Timothy McPhillips, Scott McPhillips, Ashley Deacon, Peter Kuhn and Michael Hollenbeck for helpful discussions and experimental support. This work is based upon research conducted at the Stanford Synchrotron Radiation Laboratory (SSRL). SSRL is funded by the Department of Energy (BES, BER) and the National Institutes of Health (NCRR, NIGMS).

References

Brunger, A. T., Adams, P. D., Clore, G. M., DeLano, W. L., Gros, P., Grosse-Kunstleve, R. W., Jiang, J.-S., Kuszewski, J., Nilges, M., Pannu, N. S., Read, R. J., Rice, L. M., Simonson, T. & Warren, G. L. (1998). *Acta Cryst.* D**54**, 905–921.
Brunori, M., Vallone, B., Cutruzzola, F., Travaglini-Allocatelli, C., Berendzen, J., Chu, K., Sweet, R. M. & Schlichting, I. (2000). *Proc. Natl Acad. Sci. USA*, **97**, 2058–2063.
Collaborative Computational Project, Number 4 (1994). *Acta Cryst.* D**50**, 760–763.
Djinovic Carugo, K., Everitt, P. & Tucker, P. (1998). *J. Appl. Cryst.* **31**, 812–814.
Evans, G. & Perrifer, R. F. (1996). *Rev. Sci. Instrum.* **67**, 47–53.
Kroeger, K. S. & Kundrot, C. E. (1994). *J. Appl. Cryst.* **27**, 609–612.
La Fortelle, E. de & Bricogne, G. (1997). *Methods Enzymol.* **276**, 472–494.
Leslie, A. G. W. (1999). *Acta Cryst.* D**55**, 1696–1702.
Machius, M., Henry, L., Palnitkar, M. & Deisenhofer, J. (1999). *Proc. Natl Acad. Sci. USA*, **96**, 11717–11722.
McRee, D. E. (1999). *J. Struct. Biol.* **125**, 156–165.
Merritt, E. A. & Bacon, D. J. (1997). *Methods Enzymol.* **277**, 505–524.
Perrakis, A., Sixma, T. K., Wilson, K. S. & Lamzin, V. S. (1997). *Acta Cryst.* D**53**, 448–455.
Prangé, T., Schiltz, M., Pernot, L., Colloc'h, N. & Longhi, S. (1998). *Proteins Struct. Funct. Genet.* **30**, 61–73.
Sauer, O., Schmidt, A. & Kratky, C. (1997). *J. Appl. Cryst.* **30**, 476.

Schiltz, M., Kvick, A., Svensson, O., Shepard, W., de La Fortelle, E., Prangé, T., Kahn, R., Bricogne, G. & Fourme, R. (1997). *J. Synchrotron Rad.* **4**, 287–297.
Schiltz, M., Prangé, T. & Fourme, R. (1994). *J. Appl. Cryst.* **27**, 950–960.
Schiltz, M., Shepard, W., Fourme, R., Prange, T., de La Fortelle, E. & Bricogne, G. (1997). *Acta Cryst.* D**53**, 78–92.
Schoenborn, B. P. (1969). *J. Mol. Biol.* **45**, 297–303.
Schoenborn, B. P., Watson, H. C. & Kendrew, J. C. (1965). *Nature (London)*, **207**, 28–30.
Sheldrick, G. M. (1997). *Direct Methods for Solving Macromolecular Structures*, edited by S. Fortier, pp. 119–130. Dordrecht: Kluwer Academic Publishers.
Soltis, M. S., Stowell, M. H. B., Wiener, M., Phillips, G. & Rees, D. (1997). *J. Appl. Cryst.* **30**, 190–194.
Stanford Synchrotron Radiation Laboratory (2000). *Protein Crystallography at the Stanford Synchrotron*, http://smb.slac.stanford.edu.
Stowell, M. H. B., Soltis, M., Kisker, C., Peters, J. W., Schindelin, H., Rees, D. C., Cascio, D., Beamer, L., Hart, P. J., Wiener, M. C. & Whitby, F. G. (1996). *J. Appl. Cryst.* **29**, 608–613.
Tilton, R. F. (1988). *J. Appl. Cryst.* **21**, 4–9.
Tilton, R. F., Kuntz, I. D. & Petsko, G. A. (1984). *Biochemistry*, **23**, 2849–2857.
Vacquier, V. D. & Lee, Y.-H. (1993). *Zygote*, **1**, 1–16.
Vitali, J., Robbins, A. H., Almo, S. C. & Tilton, R. F. (1991). *J. Appl. Cryst.* **24**, 931–935.